lapsed approximately into a common band in the inner region ($y^+ < 40$). An explanation for the deviation of the other two curves has not been formulated.

References

[1] Townsend, A. A., "Equilibrium Layers and Wall Turbulences," *Journal of Fluid Mechanics*, Vol. 11, Pt. 1, Aug. 1961, pp. 97–120.

[2] Bradshaw, P., Ferriss, D. H., and Atwell, N. P., "Calculation of Boundary-Layer Development Using the Turbulent Energy Equation," *Journal of Fluid Mechanics*, Vol. 28, Pt. 3, May 1967, pp. 593–616.

[3] Bradshaw, P., "The Turbulence Structure of Equilibrium Boundary Layers," *Journal of Fluid Mechanics*, Vol. 29, Pt. 4, Sept. 1967, pp. 625–645.

[4] Bradshaw, P. and Ferriss, D. H., "Calculation of Boundary Layer Development Using the Turbulent Energy Equation; IV: Heat Transfer with Small Temperature Differences," Aero Rept. 1271, 1968, National Physics Lab.

[5] Chen, T. N. and Toong, T. Y., "Laminar Boundary-Layer Wedge Flows with Evaporation and Combustion," AIAA Paper 63-449, Palm Beach, Fla., 1963.

[6] Wooldridge, C. E. and Muzzy, R. J., "Measurements in a Combusting Turbulent Boundary Layer with Porous Wall Injection," *Tenth Symposium (International) on Combustion*, the Combustion Institute, Pittsburgh, Pa., 1965.

[7] Jones, J. W., "A Turbulent Boundary Layer with Mass Addition, Combustion, and Pressure Gradient," Ph.D. dissertation, Department of Mechanical Engineering, Univ. of Utah (to be published).

Integral Method for Internal Hypersonic Flows

LEVON M. MINASSIAN*
Canadair Ltd., Montreal, Canada

Nomenclature

e = specific internal energy
M = Mach number
p = static pressure
U = freestream velocity
u = axial velocity in the shock layer
v = lateral velocity ($\perp$ to freestream) in the shock layer
x,y = nondimensional Cartesian coordinates in terms of leading-edge radius y_0
ρ = density
γ = ratio of specific heats = 1.4
ϵ = density ratio across shock, ρ_∞/ρ_s
σ = angle between shock wave and freestream

Superscripts

$'$ = first derivative with respect to x
$''$ = second derivative with respect to x
$'''$ = third derivative with respect to x

Subscripts

0 = condition at the leading edge
1 = condition at a general point
s = condition at the shock
∞ = condition at freestream
b = condition at the body

Received November 17, 1969; revision received February 26, 1970. The author expresses his gratitude to S. Mölder of McGill University for making available the results of the method of characteristics.

* Research Engineer, Technology Development—Aerodynamics.

Introduction

THE Note presents the formulation and the numerical results of an integral method, thin-shock-layer analysis. The solution is obtained by integration of a single ordinary differential equation, which determines both the shock shape and surface pressure.

Formulation of the Problem

The integral conservation equations across the shock layer may be expressed for internal axisymmetric flows between two axial stations x_0 and x_1.

Continuity:

$$\rho_\infty U(y_0^2 - y_{s_1}^2)/2 = \int_{y_{s_1}}^{y_b} \rho u y dy \quad (1)$$

Axial Momentum:

$$(p_\infty + \rho_\infty U^2)(y_0^2 - y_{s_1}^2)/2 = \int_{y_{s_1}}^{y_{b_1}} (p + \rho u^2) y dy - \int_{y_0}^{y_{b_1}} p_b y_b dy_b \quad (2)$$

Lateral Momentum:

$$\int_{y_{s_1}}^{y_{b_1}} \rho u v y dy = \int_{x_0}^{x_1} (p_\infty - p_s) y_s dx \quad (3)$$

Energy:

$$\rho_\infty U[e_\infty + (p_\infty/\rho_\infty) + U^2/2](y_0^2 - y_{s_1}^2)/2 = \int_{y_{s_1}}^{y_{b_1}} \rho u[e + (p/\rho) + (u^2 + v^2)/2] y dy \quad (4)$$

The concept of thin-shock-layer theory stipulates constancy of flow variables across the shock layer between shock and body. The pressure and the lateral velocity v are thus assumed to vary only in the axial direction. Following Chernyi[1,2] the constant pressure across the layer is assumed to be equal to its wall value p_b. The constant lateral velocity is taken equal to its value behind the shock

$$v = v_s = U y_s'(1 - \epsilon) = [2U y_s'/(\gamma + 1)][1 - 1/(M_\infty^2 y_s'^2)] \quad (5)$$

In addition, u is assumed to be equal to U. This approach is fully justified in the limit as $\epsilon \to 0$. Chernyi claims reasonably accurate results with values as high as 0.3.

The above assumptions, made by Hayes and Probstein[3] in their analysis for external flows, confine the problem to slender bodies. Two approaches will be considered to overcome this restriction.

In the first approach, Eq. (5) is determined from the continuity relationship across an oblique shock, assuming $\sin^2\sigma = y_s'^2$. This assumption underestimates the magnitude of the first and second derivatives of y_s, thus resulting in a thinner shock layer; v_s in Eq. (5) therefore is underestimated. The assumption $u \approx U$ overestimates u. For large M_∞ and inlet angles, the lowering of values of v_s is the stronger of the two effects and hence the pressure in the shock layer is expected to be overestimated. The exact form of Eq. (5) is:

$$v_s/U = 2y_s'[1 - (1 + y_s'^2)/(M_\infty^2 y_s'^2)]/[(\gamma + 1) \times (1 + y_s'^2)] \quad (6)$$

Substitute Eq. (6) in the exact form of u/U from two-dimensional oblique relations to obtain

$$u/U = 2\{[(\gamma + 1)/2] + (1/M_\infty^2) - y_s'^2/(1 + y_s'^2)\}/(\gamma + 1) \quad (7)$$

With the aid of Eq. (1) and assuming constancy of flow variables across the shock layer, Eq. (3) may be differentiated with respect to x resulting in

$$p_b/(\rho_\infty U^2) = [1/(M_\infty^2)] + (y_s' v_s/U) + (y_0^2 - y_s^2)(v_s'/U)/(2y_s) \quad (8)$$

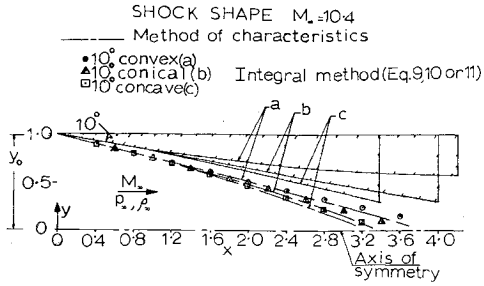

Fig. 1 Shock shapes for a) 10° convex body, b) 10° conical inlet, and c) 10° concave body ($M_\infty = 10.4$, $\gamma = 1.4$).

Using Eqs. (1, 2, and 8) and the perfect gas relations, Eq. (4) may be differentiated with respect to x. The final form of the improved equation is

$$y_s''' = (A1 - B1 + C1 + D1 + E1 - F1)/G1 \quad (9)$$

where:

$$A1 = (p_b/\rho_\infty U^2)(y_b y_b' + [(y_b^2 - y_s^2)/2]\{[1/(\gamma - 1)] \times (u'/U) + (u'/U)\} + (y_b y_b' - y_s y_s')\{(u/U)[1/(\gamma - 1)] + (u/U) - 1\})$$

$$B1 = (y_s y_s'/2)\{[(u/U) - 1]^2 + (v_s/U)^2\}$$

$$C1 = [(y_0^2 - y_s^2)/2]\{[(u/U) - 1](u'/U) + (v_s/U)(v_s'/U)\}$$

$$D1 = y_s y_s'/[\gamma(\gamma - 1)M_\infty^2]$$

$$E1 = [(y_b^2 - y_s^2)/2]\{(u/U)[1/(\gamma - 1)] + (u/U) - 1\}\{y_s'(v_s'/U) + y_s''(v_s/U) + (v_s'/U)(y_s'/2)[(y_0^2/y_s^2) + 1]\}$$

$$F1 = (y_s/2)[(y_0^2/y_s^2) - 1][(y_b^2 - y_s^2)/(\gamma + 1)] \times \{(u/U)[1/(\gamma - 1)] + (u/U) - 1\} \times \{[8y_s'^3 y_s''^2/(1 + y_s'^2)^3][1 - (1/M_\infty^2 y_s'^2)] - [2y_s' y_s''^2/(1 + y_s'^2)^2][3 + (1/M_\infty^2 y_s'^2)] - [2y_s''^2/M_\infty^2 y_s'^3(1 + y_s'^2)]\}$$

$$G1 = [y_s(y_b^2 - y_s^2)/2(\gamma - 1)(1 + y_s'^2)]\{(u/U) \times [1/(\gamma - 1)] + (u/U) - 1\}[(y_0^2/y_s^2) - 1] \times \{1 + (1/M_\infty^2 y_s'^2) - [2y_s'^2/(1 + y_s'^2)][1 - (1/M_\infty^2 y_s'^2)]\}$$

v_s/U, v_s'/U, u/U and u'/U are given by Eqs. (6) and (7) and their derivatives with respect to x; $p_b/(\rho_\infty U^2)$ is given by Eq. (8). Equation (9) is a third-order ordinary differential equation, the numerical solution of which determines the shock shape and the surface pressure. It is singular at the leading edge and the solution may therefore be started at a small distance Δx from the leading edge where the shock is assumed straight and locally two-dimensional.

As a second approach, Eq. (6) is used with the assumption $u \approx U$ retained as in Ref. 3. Proceeding as in the derivation

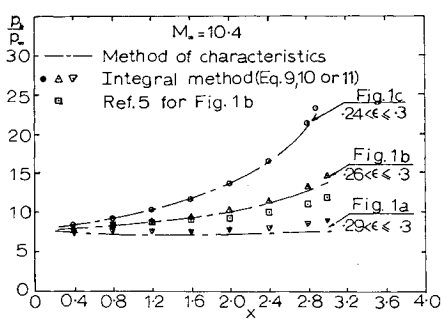

Fig. 2 Surface pressure ratios for Fig. 1 ac ($M_\infty = 10.4$, $\gamma = 1.4$).

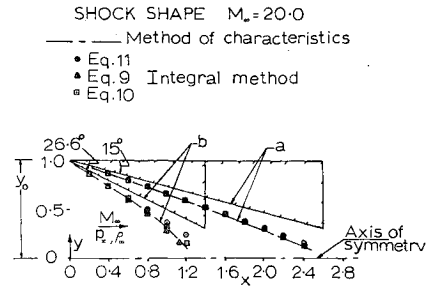

Fig. 3 Shock shapes for 15° and 26.6° conical inlets ($M_\infty = 20$, $\gamma = 1.4$).

of Eq. (9), the second improved equation is

$$y_s''' = (A2 - B2 + C2 + D2 + E2 - F2)/G2 \quad (10)$$

The terms in Eq. (10) are identical with those in Eq. (9) except for u/U, which is now assumed to be equal to unity; its derivative u'/U therefore vanishes.

For the purpose of comparison, the original approach by Hayes and Probstein, for slender bodies, may be written for internal flows as

$$y_s''' = (A - B + C + D + E - F)/G \quad (11)$$

The terms in Eq. (11) are identical with those in Eq. (10) except for v_s/U and v_s'/U, which are now given by Eq. (5) and its derivative, respectively.

Numerical Results and Discussions

Figure 1a–c refers to three inlets with relatively small surface inclinations to the freestream flow, and the results of the three Eqs. (9–11) are all identical for $M_\infty = 10.4$; 1b refers to a 10° conical inlet, Fig. 1a and 1c to inlets 10° initially. The former decreases by 1°/unit length (convex) and the latter increases by 1°/unit length (concave). The shock shapes are in good agreement with the characteristics results.[4] The surface pressure ratios (p_b/p_∞) and the range of values for $\epsilon(\rho_\infty/\rho_s)$ are shown in Fig. 2. The agreement with the characteristics solution is encouraging. The slight discrepancies in the downstream direction are due to shock-layer thickening, which violates the assumption of constancy of variables across the layer. This discrepancy is more significant in the case of Fig. 1a, with the thickest layer. The pressure distribution of the modified shock-layer theory[5] is also shown for the conical inlet. From the point of view of computing time, this method is not suitable for pressure prediction.

The more severe situations of large shock angles are illustrated in Figs. 3 and 4; 3a refers to a 15° conical inlet and Fig. 3b to a 26.6° inlet at $M_\infty = 20$. With Eq. (11) the errors in shock shape and surface pressure were predicted above. The improvement in shock geometries is noted with Eqs. (9) and

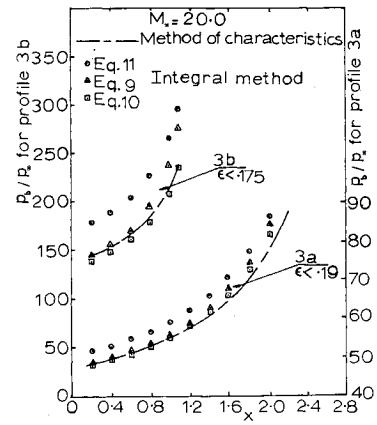

Fig. 4 Surface pressure ratios for 15° and 26.6° conical inlets ($M_\infty = 20$, $\gamma = 1.4$).

(10). The surface pressure ratios in Fig. 4a,b show a very good agreement with Eq. (9) near the leading edge. The slight underestimation with Eq. (10) is most probably due to the assumption $u \approx U$, which overestimates total velocities locally. Further downstream, as the shock wave approaches the axis of symmetry, locally two-dimensional flow can no longer be assumed and the pressures with both equations are overestimated. This effect is a disadvantage for Eq. (9) but an advantage for Eq. (10). From an over-all point of view the latter is the most reliable and it is recommended by the author.

The tendency to overestimate surface pressures toward the rear with all the three equations is due to either or both a) shock-layer thickening, and b) deviation from locally two-dimensional flow, as the shock approaches the axis of symmetry. For small $y_s'^2$ as in Fig. 1a–c, the latter effect is negligible. Furthermore, at distances downstream this situation rarely occurs because of the formation of a Mach disk followed by locally subsonic flow. The present method is inapplicable for such flow conditions.

The average execution time for each of the cases considered above was about 11 sec on an IBM computer 360/75, running in a multiprocessing environment.

References

[1] Chernyi, G. G., "Application of Integral Relationships in Problems of Propagation of Strong Shock Waves," *Journal of Applied Mathematics and Mechanics (Prikladnaia Matematika i Mekhanika)*, Vol. 24, 1960, pp. 159–165.

[2] Chernyi, G. G., "Integral Methods for the Calculation of Gas Flows With Strong Shock Waves," *Journal of Applied Mathematics and Mechanics (Prikladnaia Matematika i Mekhanika)*, Vol. 25, 1961, pp. 138–147.

[3] Hayes, W. D. and Probstein, R. F., "Hypersonic Flow Theory," *Inviscid Flows*, 2nd ed., Vol. 1, Academic Press, New York, 1966, pp. 355–366.

[4] Sorensen, V. L., "Computer Program for Calculating Flow Fields in Supersonic Inlets," TN D-2897, 1965, NASA.

[5] Lee, B. H. K., "A Modified Shock Layer Theory for Hypersonic Internal Flows," *Canadian Aeronautics and Space Institute Transactions*, Vol. 2, No. 2, Sept. 1969, pp. 67–74.

Drag Measurements on Particles in Compressible Flow by a Light Extinction Technique

FRANK T. BUCKLEY JR.*
University of Maryland, College Park, Md.

Nomenclature

C_D = particle drag coefficient
C_{DFD} = finite difference determined particle drag coefficient
E = voltage output from light detection circuit (particles present)
E_0 = voltage output from light detection circuit (no particles present)
d_p = particle diameter
k_s = extinction coefficient for scattering
k_{sa} = extinction coefficient for scattering plus absorption
l = particle cloud thickness
M = particle Mach number
Re = particle Reynolds number
S = average spacing of particles in cloud in particle diameters
t = time
Δt = time interval after shock front crosses light beam
u = cloud velocity in laboratory coordinates
u_c = cloud velocity before acceleration in laboratory coordinates
u_p = particle velocity in laboratory coordinates
u_s = primary shock velocity in laboratory coordinates
x = laboratory spatial coordinate parallel to and increasing in the direction of primary shock propagation
δ = cloud nonuniformity parameter defined below Eq. (3)
ρ = mass density of gas
ρ_p = mass density of particle cloud
ρ_s = mass density of particle material

Subscripts

1 = immediately upstream of primary shock front
2 = immediately downstream of primary shock front

Received October 20, 1969; revision received February 25, 1970.

* Assistant Professor, Department of Mechanical Engineering.

Introduction

A NUMBER of investigations have been undertaken directed towards the determination of the aerodynamic drag on clouds of μ-sized particles. Because of the many factors that can significantly affect the drag on such systems, differences between the results of various experimental studies (generally confined to particle Mach numbers below 0.4) have occurred. The majority of the more recent drag coefficient determinations have depended upon a photographic recording of a particle's displacement history during its acceleration[1–4] (usually behind the primary shock wave in a shock tube). Exceptions to these are the study conducted by the author,[5] where the particle acceleration was evaluated by a light extinction method, and that later carried out by Rudinger[6] using a similar technique.

Considering the need for more particle drag data, and noting that none have been reported in the transonic flow range, it is felt that the results of the experiments described in Ref. 5 are of interest. This Note serves to summarize the results of that study.

Experiment

An externally generated particle cloud, composed of 74–89 μ diam solid glass spheres suspended in air, was continuously injected downward into a vertically mounted shock tube from a position just below its diaphragm. The diaphragm was then ruptured causing a normal shock wave to propagate through the slowly moving cloud thereby accelerating and compressing it. Since the rate of cloud compression is a function of the drag forces that act on the particles, the particle drag coefficient could be inferred from a measurement of the cloud density history. Such a measurement was obtained by passing a parallel monochromatic light beam through the accelerating cloud in a thin plane normal to its direction of motion. This beam was attenuated by the particles (primarily due to scattering) so that it emerged with a reduced, cloud density dependent intensity. The attenuated beam was focused on the cathode of a photomultiplier tube producing an anode current that was directly related to the beam intensity. This current passed through a fixed resistive load, and the voltage drop so produced was displayed and photographically recorded on an oscilloscope. The initial pressure and initial temperature in the driven tube, together with the shock speed, were also measured in a conventional manner. The Reynolds number was varied by changing the initial pressure in the driven tube.

Analysis

The voltage output from the light detection circuit was related to the cloud density through[7]

$$E/E_0 = \exp[-(3k_{s,sa}l\rho_p)/(2\rho_s d_p)] \quad (1)$$

The data reduction equation was obtained by combining Eq. (1) with the familiar one-dimensional equations of motion for particle-gas flows.[8] Assuming 1) the particle size was uniform, 2) the shock speed u_s was constant, 3) the particles and